voltage was ~1.4 kV with a pulse length of 0.40 to 0.45 ms. Electroporated cells were incubated at room temperature for 15 min and transferred into an enriched culture medium (DMEM) (*12*) with 20% Nu serum (Collaborative Research, Inc., Bedford, MA) containing 0.04% gentamicin and incubated for 16 hours at 37°C. This material was then harvested and washed at 4°C in 0.25 M tris-HCl (pH 7.8). After resuspension in 100 μl of 0.25 M tris-HCl (pH 7.8), the cells were frozen and thawed three times. The lysate was cleared by centrifugation in an Eppendorf Microfuge (10,000*g*) for 10 min.

22. CAT activity was assayed in a mixture of 0.25 M tris-HCl (pH 7.8), 1 mM acetyl coenzyme A, 0.3 μCi of [^{14}C]chloramphenicol (50 to 60 mCi/mmol; Amersham) in a final volume of 100 μl. The reaction mix was incubated at 37°C for 16 hours, extracted with ethylacetate, and dried. The pellet was resuspended in 27 μl of ethylacetate and spotted on a thin-layer chromatography plate (PE SIL G, Whatman). After development for 2 hours with chloroform-methanol (95:5), the plates were dried and analyzed with a Phosphor Imager (Molecular Dynamics).
23. Parasites (5×10^7) were electroporated with 25 pmol of either TUB1 CAT or ROP1/2 CAT plasmids and inoculated into monolayers of HFF. One day later, lysis of the host cell was complete, and the recombinant parasites were harvested and counted. One-fifth to one-tenth (usually ~1×10^7 parasites) of the population was inoculated and expanded in HFF until they lysed again 2 days later. In parallel, cell lysates were prepared from 5×10^7 parasites and assayed for CAT activity, and total DNA was extracted from 5×10^7 parasites and subjected to Southern (DNA) blot analysis. The same procedure was repeated until day 9 after electroporation.
24. J. R. Neumann, C. A. Morency, K. O. Russian, *BioTechniques* **5**, 444 (1987).
25. Total DNA was extracted from 10^7 parasites and transferred by slot blotter, in duplicate, to nylon membranes. The presence of CAT DNA sequences was detected by Southern blot analysis with a 600-bp DNA fragment encoding the CAT sequence. Signals for each point were normalized to the same amount of total DNA with signals obtained by hybridization of the duplicate with a single-copy *Toxoplasma* gene probe. The probes were labeled by the random primer method with ^{32}P-labeled deoxycytidine 5′-triphosphate, and the spots were quantified by Phosphor Imager.
26. J. Sambrook, E. F. Fritsch, T. Maniatis, *Molecular Cloning: A Laboratory Manual* (Cold Spring Harbor Laboratory Press, Cold Spring Harbor, NY, ed. 2, 1989).
27. We thank D. Wirth, T. Soldati, and our colleagues for helpful suggestions; S. Pfeffer for use of the Phosphor Imager; and K. Kim and S. Tomavo for critical reading of the manuscript. Supported by the National Institutes of Health, the MacArthur Foundation, the Burroughs Wellcome Fund molecular parasitology award, a European Molecular Biology Organization fellowship, and a Swiss National Foundation fellowship.

20 October 1992; accepted 14 January 1993

Structure of DNA Polymerase I Klenow Fragment Bound to Duplex DNA

Lorena S. Beese,* Victoria Derbyshire,† Thomas A. Steitz‡

Klenow fragment of *Escherichia coli* DNA polymerase I, which was cocrystallized with duplex DNA, positioned 11 base pairs of DNA in a groove that lies at right angles to the cleft that contains the polymerase active site and is adjacent to the 3′ to 5′ exonuclease domain. When the fragment bound DNA, a region previously referred to as the "disordered domain" became more ordered and moved along with two helices toward the 3′ to 5′ exonuclease domain to form the binding groove. A single-stranded, 3′ extension of three nucleotides bound to the 3′ to 5′ exonuclease active site. Although this cocrystal structure appears to be an editing complex, it suggests that the primer strand approaches the catalytic site of the polymerase from the direction of the 3′ to 5′ exonuclease domain and that the duplex DNA product may bend to enter the cleft that contains the polymerase catalytic site.

The large proteolytic fragment of DNA polymerase I (Pol I) from *E. coli* [Klenow fragment (KF)] contains a 5′ to 3′ polymerase activity and a 3′ to 5′ exonuclease activity that edits mismatched bases. The two active sites that catalyze these reactions are separated by about 35 Å in the crystal structure (*1*). A specific proposal for how these sites work together to enhance the fidelity of DNA replication (*2–4*) is consistent with biochemical and kinetic observations (*5–8*). The establishment of a detailed structural basis for polymerization and editing has been hindered because it has not been possible to visualize duplex DNA bound to DNA polymerase in either the polymerase or exonuclease active site.

A cocrystal structure of KF with an 8-bp DNA duplex showed the 3′ end of a single-stranded region three nucleotides in length bound in the exonuclease active site, but no duplex DNA was seen (*4*) even though biochemical analysis of these cocrystals demonstrated a 1:1 stoichiometry of DNA:KF. Comparison of the apo-enzyme and cocrystal structures indicated that a "thumb-like" protrusion consisting of two long helices (H and I) from one side of the polymerase cleft changed conformation upon DNA binding and that the DNA was too disordered to be seen.

The catalytic site for the polymerase reaction is located at the bottom of the large cleft. This region contains a tight cluster of the most highly conserved residues in the polymerase sequences that have been aligned (*1, 9*), a binding site for the deoxynucleoside triphosphates (*10*), and residues whose mutations eliminate polymerase, but not exonuclease, activity (*11*). On the basis of the results of footprinting studies that showed protection of 8 bp of duplex product (*2, 12*) and electrostatic calculations (*13*), a primer-template model was built into the cleft, with the primer strand entering it from the end farthest from the 3′ to 5′ exonuclease active site (*1*). However, this model failed to explain several more recent observations. The location of catalytically important side chains (*11*) and the location of deoxynucleotide triphosphate (dNTP) bound in the crystal structure (*10*) position the catalytic site deeper into the cleft than had been previously suspected; this makes the placement of the 3′ end of the model-built DNA near the catalytic site sterically impossible and inconsistent with the DNA footprinting results. The location of duplex DNA in the complex reported here suggests that the primer strand enters the polymerase active site cleft from a direction opposite that in earlier models (that is, at the end of the large cleft adjacent to the exonuclease site), which obviates many of these earlier problems.

To enhance our chances of obtaining a polymerase complex, we incorporated adenosine 2′,3′ riboepoxy adenosine triphosphate (epoxyATP), which is known to produce tight binding of DNA to the polymerase site (*5*), onto the 3′ end of the primer strand. Although KF was incubated at a concentration of 10 mg/ml for 48 hours with a threefold molar excess of complementary 7- and 12-nucleotide (nt) DNA strands (*14*) and epoxyATP, an unexpected complex was obtained. The complex crystallized from a 35% saturated ammonium sulfate solution with the same space group as apo-KF but with a 1% increase in the length of the *a* and *b* axes. A difference electron density map between the complex and the apo enzyme (Fig. 1A) shows 11 bp of distorted duplex B-DNA, a 3-nt single-stranded DNA overhang with its 3′ terminal nucleotide bound at the 3′ to 5′ exonuclease active site, and one nonstandard base pair at the junction between single-stranded and double-stranded regions. The 5′ terminal nucleotide of the 12-nt strand is not base-paired and binds at the entrance to the polymerase cleft. The conformations of the four nucleotides (1 to 4) of the primer strand bound to the exonuclease active site

Departments of Molecular Biophysics and Biochemistry and Chemistry and the Howard Hughes Medical Institute, Yale University, New Haven, CT 06511.

*Present address: Department of Biochemistry, Duke University Medical Center, Durham, NC 27710.
†Present address: David Axelrod Institute of Public Health, New York State Department of Health, Wadsworth Center for Laboratories and Research, Albany, NY 12201.
‡To whom correspondence should be addressed.

are identical with those observed previously in a complex with a single-stranded tetranucleotide, $(dT)_4$ (*4*, *15*). One interpretation of the observed electron density is that the duplex DNA is composed of a 12-nt template strand complexed with two processed 7-nt strands, one in which epoxyATP was added and one in which a 3′ nucleotide was removed (Fig. 1B). This would allow formation of a double-stranded region of 11 bp (although base pair 4 is unusual) and a 3-nt, single-stranded overhang at the 3′ end of the 6-nt oligomer (*16*). Although we cannot be certain of the exact sequence of the primer strand at this point, it is of no consequence to the following discussion.

Comparison of the apo and DNA complex structures shows that a conformational change occurs in a thumb-like region of the protein that makes direct contacts with the duplex portion of the DNA (Figs. 2 through 4). Residues 558 to 637, including two long helices, H and I (Fig. 3B), move toward the 3′ to 5′ exonuclease domain to interact with the DNA. Motion is the greatest, about 12 Å, for the residues near the NH_2-terminus of helix I (Figs. 2 and 4). This same motion was observed in the earlier DNA cocrystals (*4*) and in cocrystals of KF and DNA grown under low ionic strength conditions and in a different space group (*17*). In both crystal forms, the duplex DNA was disordered. The DNA-induced conformational change in KF produces an obvious second cleft between the thumb and the exonuclease domain into which the duplex DNA binds (Figs. 2B and 3A). This cleft (cleft 2 in Fig. 2B) runs at nearly right angles to the originally seen cleft that contains the polymerase active site (cleft 1 in Fig. 2B).

The region of the protein that connects helices H and I, which has been referred to previously as the "disordered domain" because the original electron density maps showed little density that was interpretable there (*1*), is more ordered in this complex and is visible. This region (Fig. 3B) consists of two helices (H_1 and H_2), two "strands"

Table 1. Amino acid side chains interacting with phosphates of DNA. Many of the amino acid residues interacting with DNA are identical or highly conserved in alignments of the six polymerases comprising the Pol I polymerase family (*9*); several residues are identical or highly conserved in all DNA polymerases aligned (*19*). The number of polymerases in which a residue is invariant is indicated in boldface. Nucleotides comprising the primer strand (6 nt + 8 nt) are numbered from the 3′ nucleotide that is bound at the 3′ to 5′ exonuclease active site, whereas nucleotides comprising the template strand (12 nt) are numbered from the 5′ end as in Fig. 1B.

Nucleotide	Residue	Comments
	Primer strand	
1 to 4	Residues identical to previous complex with $(dT)_4$ (*16*)	
5	Asn^{675}	Conserved in Pol I family (**5**)
6	Asn^{678}	Conserved in Pol I family (**4**)
	Lys^{635}	Conserved in Pol I family (**6**) Invarient in all DNA polymerases (*19*) Implicated in DNA binding (*20*)
7	Arg^{631}	Conserved in Pol I family (**4**)
	Glu^{611}	Interaction with main chain amide
8	Thr^{609}	Conserved in Pol I family (**4**)
	Template strand	
3	Arg^{835}	Conserved in Pol I family (**4**)
4	Asp^{827}	
10	Ser^{582}	Invarient in all DNA polymerases (*19*, *35*)
11	Asn^{579}	Conserved in all DNA polymerases (*19*, *35*)

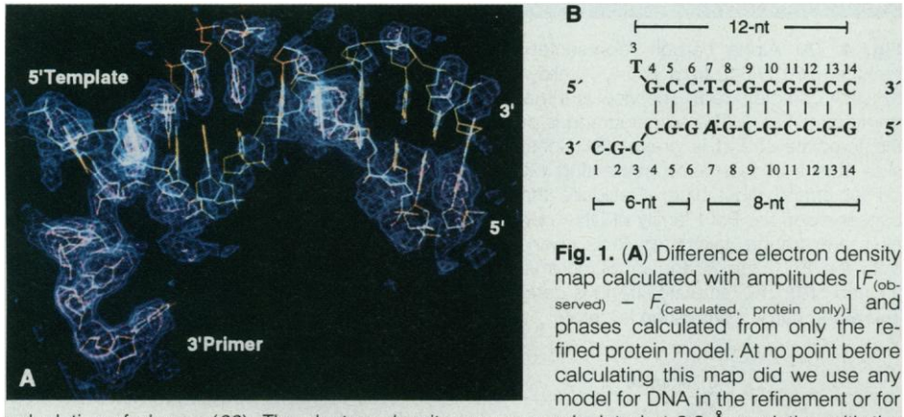

Fig. 1. (**A**) Difference electron density map calculated with amplitudes [$F_{(observed)} - F_{(calculated,\ protein\ only)}$] and phases calculated from only the refined protein model. At no point before calculating this map did we use any model for DNA in the refinement or for calculation of phases (*33*). The electron density map was calculated at 3.2 Å resolution with the program X-PLOR (*32*) and contoured at 2σ (blue) and 3σ (pink) (where σ is the SD). The *R* factor of the protein model without DNA was 23%, calculated between 10 and 3.2 Å resolution with a 0.018 Å root-mean-square deviation in bond lengths and 2.7° deviation in bond angles from ideality. The electron density is consistent with 11 bp of duplex DNA, three single-stranded nucleotides at the 3′ end bound at the 3′ to 5′ exonuclease active site, and one unpaired nucleotide on the 5′ end of the template strand (not shown). Density for this 5′ terminal nucleotide appears at lower contour in this map and is more apparent in electron density maps calculated after refinement. (**B**) Possible interaction of added oligonucleotides accounting for the electron density in (A). Perhaps the 12-nt template and 8-nt primer strands anneal as anticipated, but in addition a second 6-nt primer arising from exonuclease activity binds with its 5′ end adjacent to the 3′ end of the 8-nt strand. The base pair in position 4 is somewhat distorted. *A**, epoxyATP.

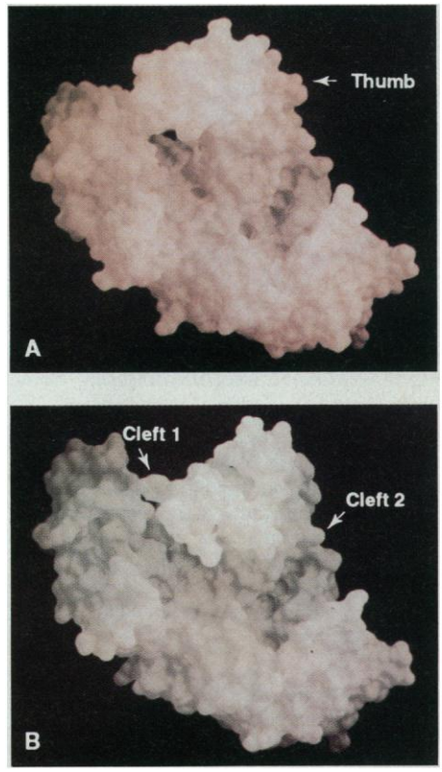

Fig. 2. (**A**) Representation of the solvent-accessible surface (*34*) of apo-KF. Compare the positions of the thumb subdomain (upper right) here with its position in (B). (**B**) Representation of the solvent-accessible surface of KF structure when bound to DNA; DNA has been omitted to show the protein structure. Cleft 1 contains the polymerase active site; cleft 2 is formed upon binding duplex DNA, which it contains.

connecting H_1 and H_2, and a loop connecting H_2 back to I. It is still not possible to fit with certainty all of the side chains in this region and, in addition, we still cannot account for 11 residues.

Contacts between the protein and duplex DNA are made exclusively through protein interactions with the DNA phosphate backbone (Fig. 4 and Table 1), consistent with the requirement that the enzyme binds any DNA independent of its sequence. In addition, the NH_2-terminus of helix H_1 fits into the minor groove of the DNA duplex, perpendicular to the DNA helix axis and similar to the helix in the GAL4 structure that interacts with the minor groove of DNA (*18*).

All of the interactions made to the primer strand are with residues that are either highly conserved in the Pol I family or to a main chain amide (Table 1) (*19*). Lys^{635}, which interacts with the primer strand in this complex, is invariant among all Pol I–like polymerases and, according to one sequence alignment, is also invariant among all eukaryotic, alpha-like DNA polymerases (*19*). Chemical modification studies indicate that Lys^{635} is directly involved in DNA binding (*20*). That the most highly conserved residues in the thumb subdomain are seen in contact with duplex DNA (Table 1) serves both to support the relevance of this observed complex to polymerase and exonuclease activity and to provide a functional and structural rationale for the conservation of these residues.

Although the DNA in these crystals is in an editing complex, its position has important implications for the mode of DNA binding at the polymerase active site because the primer terminus can move from one active site to the other without dissociation (*6*). Figure 5 portrays models for both the editing and polymerizing complexes based on the observed complex crystal structure. The editing complex is modified from the crystal structure to include a template strand extended on its 5′ end, which we propose binds in the polymerase cleft. The model of the polymerizing complex additionally postulates that the primer strand is base-paired to the template in the polymerase cleft and that its 3′ terminus is near the divalent metal ions that bind to the catalytically important Asp^{882}, Glu^{883}, and Asp^{705} (*21*). Some distortion of the duplex primer terminus or motion of the protein would be required because of the narrowness of the observed cleft. This placement of the primer strand necessarily places much of the template strand at the primer terminus in contact with the helical domain that forms the wall of the cleft opposite the thumb subdomain. Although the DNA lies within the polymerase cleft as in the original model, the postulated direction of DNA synthesis is opposite. The duplex DNA that contains the primer terminus lies on the side of the cleft proximal to the exonuclease domain, and the single-stranded template strand enters from the distal end of the cleft (Fig. 5).

This model is consistent with the location of the catalytic residues defining the polymerase active site (*11*), the observed location of bound dNTP (*10*), and the observation that a 19- to 20-nt fragment of template interacts with the protein molecule (*22*). This orientation of the primer strand relative to the polymerase active site is also consistent with the model of DNA built on the structure of human immunodeficiency virus reverse transcriptase (HIV RT) (*23*) and with an electron density map (7 Å

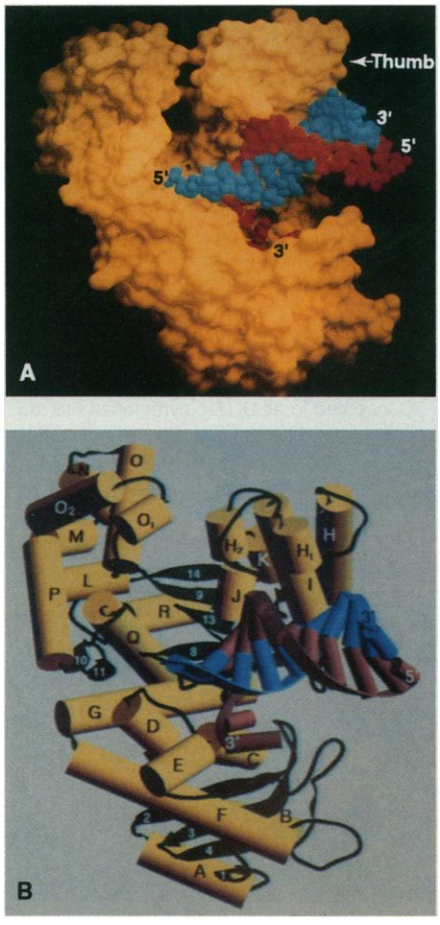

Fig. 3. (**A**) Representation of the solvent-accessible surface (*34*) of the Klenow fragment (yellow) with bound DNA. The 12-nt template strand is blue and the 14-nt primer strand is red. (**B**) Tube and arrow representation of KF in about the same orientation as (A). Helices and sheets are named as in figure 1 in (*1*). New regions of secondary structure (helices O_1 and O_2 and H_1 and H_2) were added on the basis of refined apo-KF (*21*).

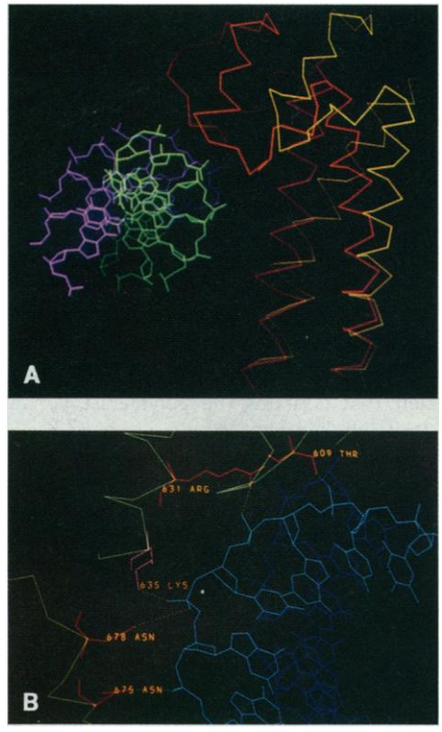

Fig. 4. (**A**) Alpha carbon representation of residues 550 to 640 from apo-KF (yellow) and KF:DNA complex (red). The view is turned 90° from that in Fig. 3. The primer strand is purple; the template strand is green. (**B**) Conserved side chains of the thumb interacting with the primer strand (light blue). Residues that are conserved in the Pol I family of DNA polymerases are orange. Lys^{635} (pink) is invariant in both the Pol I family and in all polymerases aligned (*19*). The template strand is dark blue. The alpha carbon backbone is green.

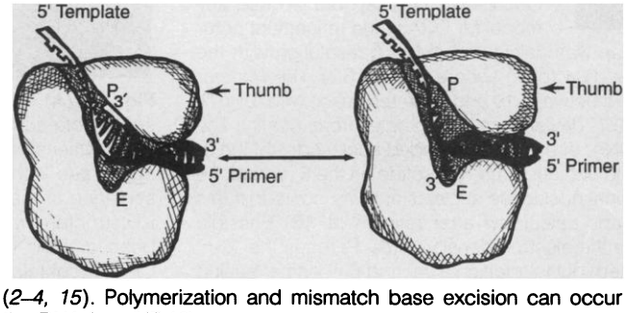

Fig. 5. A model for DNA bound at the polymerase active site P (left) and at the 3′ to 5′ exonuclease active site E (right). The portion of the DNA observed in the crystal structure is indicated in solid black and that which is model-built is in outline. The 3′ terminus of the DNA primer is proposed to shuttle between each active site (*2–4, 15*). Polymerization and mismatch base excision can occur without or with dissociation of the DNA from KF (*6*).

resolution) of HIV RT complexed with duplex DNA (*24*). Within the intrinsic limitations of the experiments, our model is not inconsistent with most of the results describing DNA binding to KF (*5, 7, 8, 25*).

The angle of the DNA helix axis in cleft 2 with respect to the polymerase cleft (cleft 1) is unexpected. If one constructs a model that preserves most of the observed contacts between the duplex DNA and the protein, the model-built DNA requires a bend of about 80° to enter the polymerase cleft (Fig. 5). Such protein-induced bending of duplex DNA is not unknown. The crystal structure of a catabolite gene activator protein–DNA complex shows that the DNA is bent by 90°, which is achieved primarily through two sharp, 43° kinks (*26*). Several recent electron microscopy studies suggest that DNA is greatly bent (as much as 180°) when bound to RNA polymerase (*27*) as well as to UvrB (*28*).

We anticipate that the growing nascent strand of the DNA substrate can shuttle between the polymerase and the exonuclease active sites (Fig. 5), as has been previously proposed (*2–4, 29*) and for which there is some evidence (*6*). The destabilization of duplex DNA that would result from the anticipated DNA bending at the polymerase active site would make the equilibrium between single- and double-stranded DNA at the primer terminus more sensitive to mismatched base pairs. It will be interesting to see whether those DNA polymerases that do not contain an editing function bind straight duplex DNA, as does HIV RT (*23, 24*), whereas those with an editing exonuclease bind bent DNA, as appears likely with DNA Pol I.

REFERENCES AND NOTES

1. D. L. Ollis *et al.*, *Nature* **313**, 762 (1985); D. L. Ollis *et al.*, *ibid.*, p. 818.
2. C. M. Joyce and T. A. Steitz, *Trends Biochem. Sci.* **12**, 288 (1987).
3. T. A. Steitz *et al.*, *Cold Spring Harbor Symp. Quant. Biol.* **52**, 465 (1987).
4. P. S. Freemont *et al.*, *Proc. Natl. Acad. Sci. U.S.A.* **85**, 8924 (1988).
5. M. Cowart *et al.*, *Biochemistry* **28**, 1975 (1989).
6. C. M. Joyce, *J. Biol. Chem.* **264**, 10858 (1989).
7. C. E. Catalano, D. J. Allen, S. J. Benkovic, *Biochemistry* **29**, 3612 (1990).
8. C. R. Guest *et al.*, *ibid.* **30**, 8759 (1991).
9. M. Delarue *et al.*, *Protein Eng.* **3**, 461 (1990).
10. L. S. Beese, J. M. Friedman, T. A. Steitz, in preparation.
11. A. H. Polesky *et al.*, *J. Biol. Chem.* **265**, 14579 (1990); A. H. Polesky *et al.*, *ibid.* **267**, 8417 (1992).
12. C. M. Joyce, unpublished data.
13. J. Warwicker, D. Ollis, F. M. Richards, T. A. Steitz, *J. Mol. Biol.* **186**, 645 (1985).
14. The sequences of the DNA oligonucleotides co-crystallized with KF are

    5′-TGCCTCGCGGCC-3′

    3′- GCGCCGG-5′

    Complementary 7-nt and 12-nt strands of DNA were annealed and incubated with a fivefold excess of 2′,3′ epoxyATP in a 3:1 molar ratio of DNA to protein under previously described conditions (*7*). The protein concentration in the reaction mixture was 10 mg/ml. The reaction mixture was incubated for 2 days at 10°C. The complex was crystallized at 17°C by vapor diffusion of a solution (10 to 12 mg/ml) of KF containing from 35 to 40% (w/v) saturated ammonium sulfate, 200 mM citrate buffer (pH 6.8), 20 mM $MgSO_4$, and 1 mM $ZnSO_4$ against a solution that was double in the concentration of all compounds except the KF:DNA complex. Crystals appeared after 6 to 8 weeks. A mutant protein [Asp^{355} → Ala (D355A)] with reduced 3′ to 5′ exonuclease activity (*30*) was used to reduce the possibility that the exonuclease would degrade the DNA in the cocrystals. The observed structure is isomorphous with the wild-type enzyme except at the exonuclease active site, where one of the two metal ions essential for exonuclease activity fails to bind. The remaining metal ion is the one that was not observed previously in a substrate complex because the D424A mutant was used to prevent substrate hydrolysis. Its position relative to the substrate is as had been expected from the positions of the two metal ions in the nucleoside monophosphate product complex (*15, 30*).
15. L. S. Beese and T. A. Steitz, *EMBO J.* **10**, 25 (1991).
16. An alternative interpretation of the two 7-nt molecules complexed to a 12-nt molecule results in a GT base pair at position 7 and a CC mismatch at position 5, where the electron density shows a good base pair. DNA from crystals used in the x-ray data collection were labeled with ^{32}P and analyzed by electrophoresis on denaturing gels. DNA lengths between 5 and 12 nt were observed, which suggests that some nuclease and polymerase processing of the DNA occurred.
17. J. M. Friedman, L. S. Beese, T. A. Steitz, unpublished data.
18. R. Marmorstein *et al.*, *Nature* **356**, 408 (1992).
19. L. Blanco *et al.*, *Gene* **100**, 27 (1991).
20. S. Basu *et al.*, *Biochemistry* **27**, 6710 (1988).
21. L. S. Beese and T. A. Steitz, in preparation.
22. T. I. Kolocheva *et al.*, *FEBS Lett.* **248**, 97 (1989).
23. L. A. Kohlstaedt, J. Wang, J. M. Friedman, P. A. Rice, T. A. Steitz, *Science* **256**, 1783 (1992).
24. E. Arnold *et al.*, *Nature* **357**, 85 (1992).
25. C. E. Catalano and S. J. Benkovic, *Biochemistry* **28**, 4374 (1989).
26. S. C. Schultz, G. C. Shields, T. A. Steitz, *Science* **253**, 1001 (1991).
27. B. ten Heggeler-Bordier, W. Wahli, M. Adrian, A. Stasiak, J. Dubochet, *EMBO J.* **11**, 667 (1992).
28. Q. Shi, R. Thresher, A. Sancar, J. Griffith, *J. Mol. Biol.* **226**, 425 (1992).
29. D. Brutlag and A. Kornberg, *J. Biol. Chem.* **247**, 241 (1972).
30. V. Derbyshire *et al.*, *EMBO J.* **10**, 17 (1991).
31. A. P. Xuong, S. T. Freer, R. Hamlin, D. Neilsen, W. Vernon, *Acta Crystallogr. A* **34**, 289 (1978).
32. A. T. Brunger, *X-PLOR Manual 2.0* (1990).
33. X-ray diffraction data were measured with a Xuong-Hamlin Mark II two-dimensional, position-sensitive area detector (*31*). The data are 87% complete to 3.2 Å, with a merging residual index (*R*) factor of 5.2%. The protein phases were obtained by rigid body refinement with the use of X-PLOR (*32*); phases were from the independently refined atomic model of the KF:DNA cocrystal in which DNA was disordered and not visible in the electron density maps although the conformational change in the thumb subdomain was observed (L. S. Beese and T. A. Steitz, unpublished data) followed by constrained positional refinement.
34. M. L. Connoly, *J. Mol. Graphics* **3**, 19 (1985).
35. There is a break in the electron density defining the main chain in this region, so it is difficult to be certain of the amino acid sequence. The electron density does not unambiguously determine which side chains are interacting with the DNA.

36. We thank M. Cowart for the generous gift of epoxyATP, C. M. Joyce and J. M. Friedman for continued help and discussions, J. Wang for assistance with Fig. 3B, and N. Hamaguchi for assistance with Fig. 5. Supported by American Cancer Society grant NP-421 to T.A.S. V.D. was supported by NIH grant GM28550 to N. Grindley.

2 November 1992; accepted 12 February 1993

Preferential Migration of Activated CD4$^+$ and CD8$^+$ T Cells in Response to MIP-1α and MIP-1β

Dennis D. Taub, Kevin Conlon, Andrew R. Lloyd, Joost J. Oppenheim, David J. Kelvin

Recombinant human macrophage inflammatory protein–1α (rhMIP-1α) and rhMIP-1β were potent chemoattractants of human T lymphocytes. These rhMIP-1 cytokines attracted only T cells activated by monoclonal antibody to CD3 and did not attract unstimulated lymphocytes. Phenotypic analysis revealed that CD4$^+$ T cells were capable of migrating in response to rhMIP-1β, whereas rhMIP-1α induced chemotaxis of predominantly CD8$^+$ T lymphocytes. Activated naïve and memory T cells also migrated in response to rhMIP-1 cytokines. Furthermore, these cytokines enhanced the ability of T cells to bind to an endothelial cell monolayer. These results suggest that rhMIP-1 cytokines preferentially recruit specific T cell subsets during the evolution of the immune response.

The accumulation of leukocytes at sites of inflammation is induced by the local production and secretion of chemotactic ligands by a wide variety of stimulated cell types. Recently, several host-derived cytokines (chemokines) have been identified that stimulate chemotaxis in vitro and elicit the accumulation of various types of inflammatory cells in vivo (*1*). Neutrophils are preferentially induced to migrate by interleukin-8 [IL-8, also called neutrophil attracting peptide–1 (NAP-1)], melanoma growth stimulating activity (MGSA, also called GRO), NAP-II, and ENA-78, whereas monocytes are preferentially in-

D. D. Taub, A. R. Lloyd, J. J. Oppenheim, D. J. Kelvin, Laboratory of Molecular Immunoregulation, Biological Response Modifier Program, National Cancer Institute, Frederick Cancer Research and Development Center (FCRDC), Frederick, MD 21702.
K. Conlon, Laboratory of Experimental Immunology, Biological Response Modifier Program, National Cancer Institute, FCRDC, Frederick, MD 21702.